PHILOSOPHICAL TRANSACTIONS A

A microstructural model of cross-link interaction between collagen fibrils in the human cornea

A. Pandolfi[1], A. Gizzi[2] and M. Vasta[3]

[1]Dipartimento di Ingegneria Civile ed Ambientale, Politecnico di Milano, Piazza Leonardo da Vinci 32, Milan, Italy
[2]Department of Engineering, University Campus Bio-Medico of Rome, Via A. del Portillo 21, Rome 00128, Italy
[3]Dipartimento INGEO, Università di Chieti-Pescara, Viale Pindaro 42, Pescara, Italy

AP, 0000-0002-7084-7456

Research

Accepted: 15 January 2019

One contribution of 11 to a theme issue 'Rivlin's legacy in continuum mechanics and applied mathematics'.

Subject Areas:
computational mechanics, mechanical engineering, structural engineering

Keywords:
collagen, microstructure, cornea, keratoconus, parametric analysis

Author for correspondence:
A. Pandolfi
e-mail: anna.pandolfi@polimi.it

We propose a simplified micromechanical model of the fibrous reinforcement of the corneal tissue. We restrict our consideration to the structural function of the collagen fibrils located in the stroma and disregard the other all-important components of the cornea. The reinforcing structure is modelled with two sets of parallel fibrils, connected by transversal bonds within the single fibril family (inter-cross- link) and across the two families (intra-cross-link). The particular design chosen for this ideal structure relies on the fact that its ability to sustain loads is dependent on the degree of the cross-link and, therefore, on the density and stiffness of the bonds. We analyse the mechanical response of the system according to the type of interlacing and on the stiffness of fibres and bonds. Results show that the weakening of transversal bonds is associated with a marked increase of the deformability of the system. In particular, the deterioration of transversal bonds due to mechanical, chemical or enzymatic reasons can justify the loss of stiffness of the stromal tissue resulting in localized thinning and bulging typically observed in keratoconus corneas.

This article is part of the theme issue 'Rivlin's legacy in continuum mechanics and applied mathematics'.

1. Introduction

The cornea is the external convex–concave lens of the eyeball that sustains the intraocular pressure (IOP) exerted by the filling fluids. Structurally, the cornea is a spherical shell made of many parallel layers. The thick central layer, the stroma, is reinforced with collagen fibrils to accomplish a load carrying function. The thinner layers regulate the transport of oxygen, nutrients, fluids and ions and protect the interior parts of the eye [1]. With an average refractive power of 43 diopters, the cornea plays the role of the principal lens of the eye system for the deviation the rays of light onto the retina to provide accurate vision. Modifications of the lens shape affect the formation of images on the retina and compromise vision.

It is acknowledged unanimously that the preservation of a stable spherical shape is due to the complex architecture of the collagen fibril network of the stroma. Collagen fibrils, embedded in a homogeneous matrix of proteoglycans and elastin, confer significant mechanical stiffness and strength to the stroma. The arrangement of the fibrils is characterized by a marked orthogonal nasal–temporal (NT) and superior–inferior (SI) pattern in the central part of the cornea and by a circumferential and radial organization along the limbus region [2].

Keratoconus is a progressive disorder and a non-inflammatory condition of the cornea that alters dramatically the shape of the lens from spherical to conical through a localized thinning [3]. The main refractive consequences of keratoconus are irregular astigmatism, strong myopia and a marked loss of vision. Macroscopically, while healthy corneas are characterized by a rather uniform or smoothly changing curvature, keratoconic corneas present a more conical shape, with abrupt changes of curvature that cause ruptures of the endothelium and trigger anomalous deposition of chemical species between the layers [4]. Keratoconus is associated with degenerative and irreversible changes in the organization of the collagen architecture [5,6] and with modifications in the chemical composition of the stroma [3].

The aetiology of keratoconus has not been clarified yet, although various hypotheses of different nature (chemical, genetic and mechanical) have been proposed and several alternatives or combined causes are under investigation. In the clinical practice, various surgical procedures have been used for the treatment of keratoconus, from corneal transplant [7] to insertion of intrastromal strengthening devices [8], to lamellar keratoplasty [9], to therapeutic cross-link [10,11].

The particular microstructure of the stroma reinforcement suggests that in keratoconus the macroscopic changes of the geometry are related to the weakening of the chemical bonds (cross-link) between the collagen fibrils [6]. Corneal fibrils are organized in ribbon-like structures called lamellae that assume an optimal configuration [2,12,13] in order to accomplish several tasks: (i) a fraction of the fibrils are randomly dispersed in all directions of the mid-surface of the cornea to provide a general confinement to the IOP; (ii) in the central cornea a portion of fibrils (about 40%) is aligned in the orthogonal SI and NT directions to provide support to the eyelid opening and closure and to the action of the muscles that rotate the eyeball; and (iii) fibrils show a circumferential and radial organization at the limbus to accommodate the transition between cornea and sclera tissues.

Since 2005, the particular collagen architecture of the stroma has been accounted for in several numerical models used in advanced biomechanical simulations, cf. the pioneering works of [14,15] and the following literature [16–24]. Most models are continuums and describe the cornea as a fibre reinforced tissue, where an isotropic matrix, obeying standard hyperelastic behaviours such as Mooney-Rivlin [25], is embedded with one or two sets of spatially distributed fibres. In the approach proposed in [26], the two sets of dispersed fibres model the sub-parallel collagen fibrils and the interlacing between lamellae, there referred to as cross-links.

Yet microstructural models of the cornea are not sufficiently advanced to be predictive in the case of diseased corneas. Simulations reported in the literature describe keratoconus by reducing the stiffness of fibrils and matrix within a portion of the cornea arbitrarily [15] or reducing the local corneal thickness [27], or including a gradual reduction both in the thickness and in the material properties [28]. More recent models are constructed from imaging and are extremely accurate

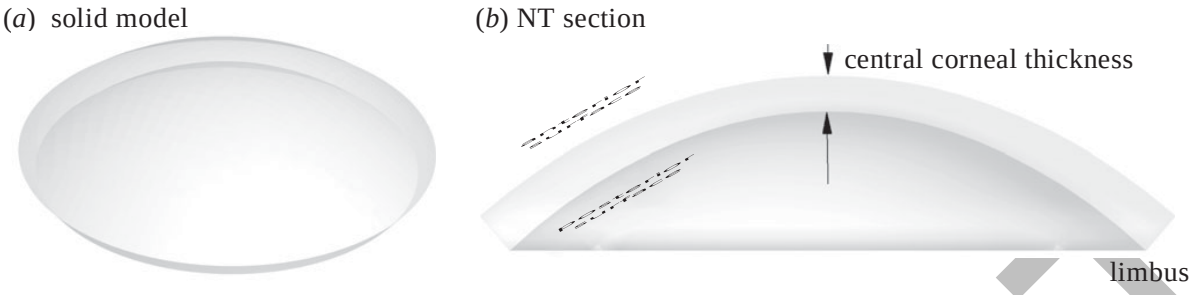

Figure 1. Geometry of the patient-specific cornea considered in this study. (*a*) Three-dimensional view. (*b*) NT meridional section with indication of the geometrical parts used for the construction of the collagen model.

from the geometrical point of view [29]; still, published models do not account for microstructural changes connected to the disease.

In the view of developing a physically based model of keratoconus that can potentially account for its onset and progression, in this study, we present a simplified model of the underlying collagen microstructure of the human cornea. The model consists of a trusswork that includes the two main sets of fibrils observed in the cornea and the hypothesized cross-links connecting the fibrils. The model disregards the actual stochastic nature of the fibril distribution, the spatial organization and regularity of collagen necessary to ensure transparency and to allow the transmission of the light, the presence of hierarchical structures forming lamellae and the mechanical contribution of the matrix components. Clearly, the model does not pretend to deliver a quantitative estimate of the deformation and the stress within a keratoconus cornea. Our goal is to understand the function of the different components of the fibril network in the preservation of the quasi-spherical configuration of the cornea.

The paper is organized as follows. Material model and numerical methods are described in §2. Numerical results are collected in §3. A discussion on the proposed model, pointing out its significance and its limits, is reported in §4.

2. Micromechanical model of the collagen network

The microstructural model of the collagen reinforcement has been constructed from the geometry of the patient-specific cornea visualized in figure 1. The anterior surface has two principal curvature radii of 7.52 mm (steepest meridian) and 7.90 mm (flattest meridian). The posterior surface has two principal curvature radii of 6.77 mm (steepest meridian) and 6.97 mm (flattest meridian). The axis of the steepest meridian is inclined of 128 degrees with respect to the NT meridian. The asphericity coefficient for both principal meridians is −0.15. The in-plane diameter of the anterior surface is 11.24 mm, and the elevation of the apex (at the centre of the cornea) is
2.54 mm. Figure 1*b* indicates the limbus, anterior and posterior surfaces, and the central corneal thickness (0.5 mm).

The micromechanical architecture of the collagen fibrils is constructed on the basis of the well-known results of *ex vivo* X-ray imaging of the human cornea [2,30], cf. figure 2*a*, disregarding the variability of such structures across the thickness that has been pointed out recently, cf. [12]. Two sets of fibrils are assumed to be aligned at the centre of the cornea, where they follow an orthogonal pattern in the NT and SI directions. At the periphery, fibrils are assumed to be aligned in an orthogonal organization parallel and perpendicular to the limbus circumference, see figure 2*b*, cf. [18,19].

The model accounts for five sets of trusses. The first two sets (F1 and F2) describe the collagen fibrils, and they are assumed to lay down on the anterior and posterior surface of the cornea. The two sets are separated by a small amount corresponding to the cornea thickness, see figure 3*a*, and the chosen discretization allows one to define the topology of a hexahedron which is considered as the basic unit cell. The third and fourth networks, parallel to F1 and F2, model the inter-fibril

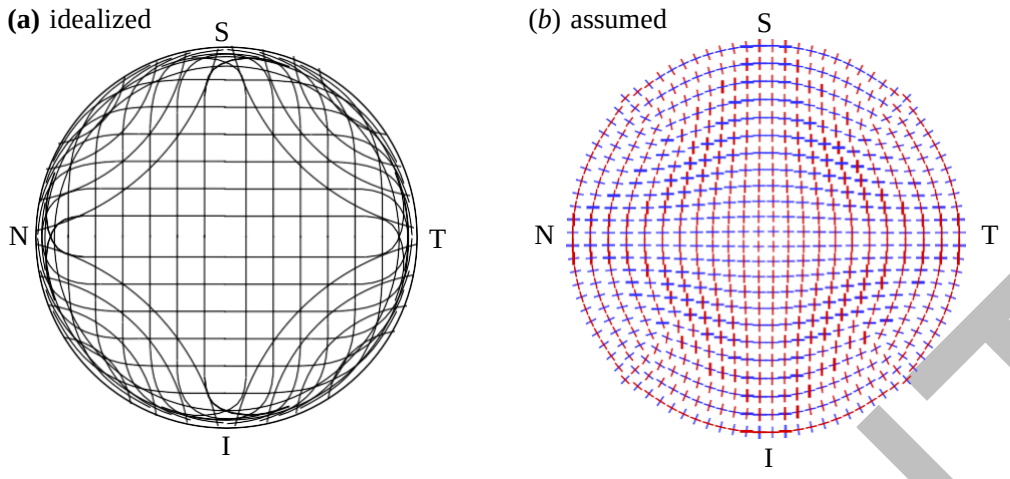

Figure 2. (*a*) Commonly accepted ideal distribution of the fibril organization within the cornea, cf. [2] and [30]. S denotes the superior point, I the inferior point, N the nasal point and T the temporal point. (*b*) Orientation of the two fibril families assumed in the structural model. The two families have the same equivalent stiffness. (Online version in colour.)

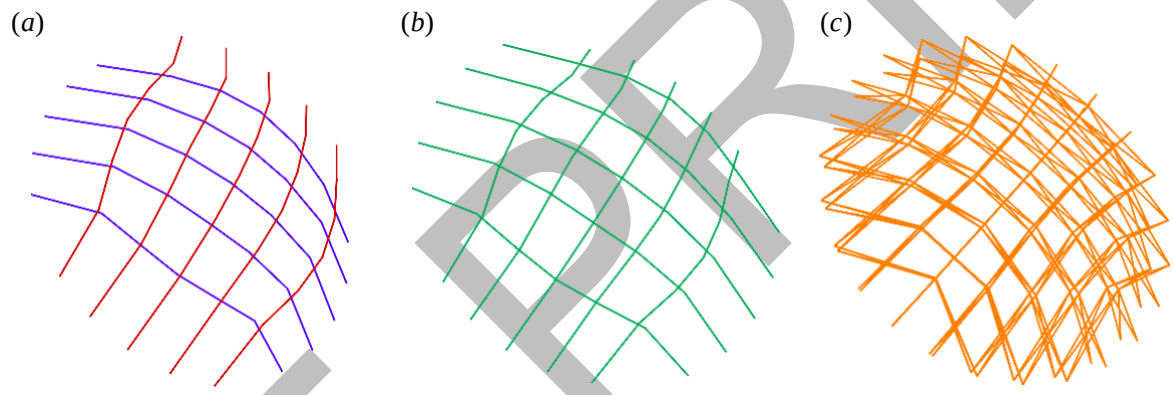

Figure 3. Schematic of the network of trusses representing the collagen fibril networks and the inter-fibril and intra-fibril cross-link networks considered in the model. (*a*) Two networks of fibrils (F1 red and F2 blue), arranged into an orthogonal structure. The two networks are displaced of a small amount to account for the actual corneal thickness. (*b*) Two networks of trusses C1 and C2 arranged to describe the inter-fibril cross-links. The first network connects the fibrils of the anterior surface, the second connects the fibrils of the posterior surface. (*c*) Network of trusses C12 describing the intra-fibril cross-links, disposed at 45 degrees between the two sets of fibrils. (Online version in colour.)

connections (inter-cross-links C1 and C2) that allow the fibrils to organize themselves in parallel sheets (lamellae). They are designed as trusses connecting the fibrils of the same network with non-parallel side links (figure 3*b*). The fifth network (C12) describes the intra-fibrils connections (intra-cross-links) between the two sets of fibrils. These trusses connect the fibrils of the anterior and the posterior lamellae along sub-diagonal directions to provide mechanical stability of the system (figure 3*c*).

We remark that the model neglects the actual spatial dispersion of the fibrils, but the assumed main orientation of the fibrils reflects faithfully the collagen microstructure averaged across the thickness. In particular, the main orientation of the fibrils switches smoothly from the NT and SI orthogonal organization at the centre to a circumferential and radial orthogonal organization at the periphery [13]. At the limbus, the majority of the fibrils runs circumferentially in the posterior third of the thickness, but fibrils assume the main radial orientation in the anterior third of the thickness. Clearly, the orthogonal structure of fibrils observed at limbus is fundamental for the mechanical stability of the system, to avoid the development of localized large deformations in the radial direction.

(*a*) unit cell (*b*) assembled network

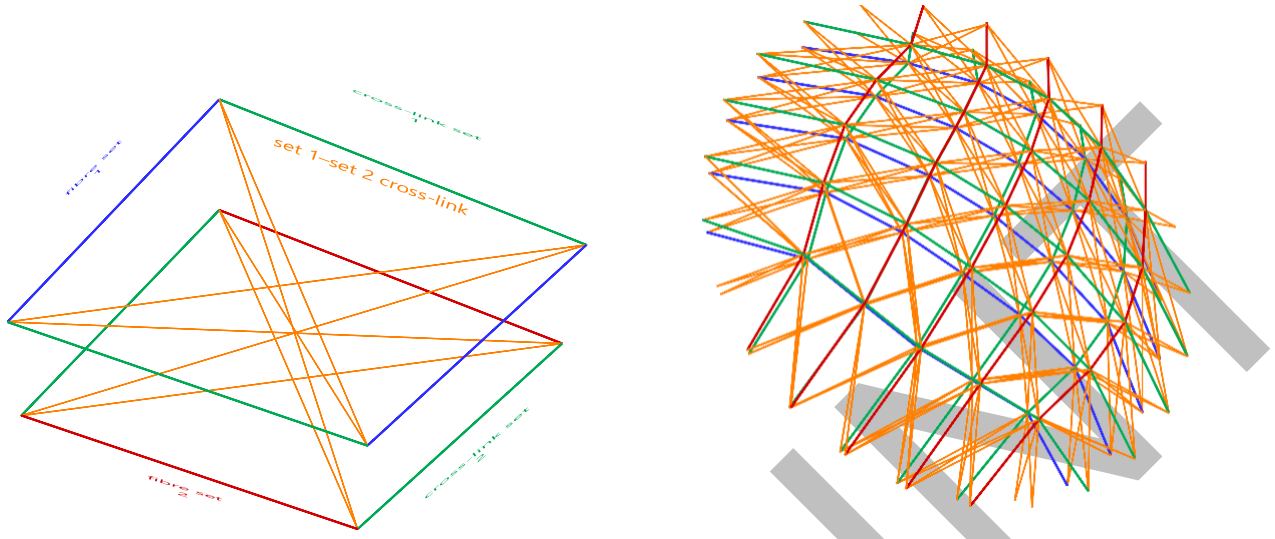

Figure 4. (*a*) Detail of the cross-links between the fibrils of the same set (inter-link, green) and of two different sets (intra-link orange). (*b*) Coarse model of the assembled trusswork including all fibril and cross-link trusses.

Figure 4*a* shows the details of an elementary cell of the model and the multiple connections. The assembled model is visualized in figure 4*b*. All trusses are connected with hinges and are assumed to be able to transmit only axial loads. In contrast with cables, trusses are able to work either in tension or compression, and the individual stress state of each element is defined by equilibrium and compatibility conditions.

Figure 4*b* visualizes a very coarse model to understand the connections between the various components. Figure 5 shows the fine model that has been used in the following static calculations, conducted with an in-house software developed specifically for this study. Note that the geometry of the trusswork has been directly derived from the finite-element discretization that we always use in continuum models of the cornea [15,19,31] (figure 5*a*). The trusswork includes 48 sub-parallel fibrils for each set, 5000 nodal points and 28 600 trusses (figure 5*b*). The distance between the anterior and posterior surface of the model is taken to be 0.3 mm, inferior to the average thickness of the cornea (0.5 mm). We remark that the model is statically stable also for zero thickness, and the distance between the anterior and posterior surface is considered only to obtain a more realistic shape in the keratoconus case. In fact, it is commonly observed that keratoconus corneas are much thinner in the zone of the conus, and the possibility to fold into an acute cone shape is also dependent on the reduced thickness. Clearly, an increase of the thickness increases the global stiffness of the model; therefore, to maintain the number of parameters at the minimum, we decided to use the same thickness also for the normal corneas.

Preliminary calculations showed that, for a fixed thickness, the solution of the simplified model in terms of displacements corresponds to the solution of the corresponding three-dimensional finite-element model, with an error less than 1%. Therefore, the discretization affects the solution in the same amount as in any linear elastic finite-element approximation.

The hinges of the trusses resting on the external ring, corresponding to the limbus, are pinned. In keeping with the trusswork theory, where body and surface loads cannot be considered, IOP is described in terms of point loads applied to the hinges (nodes) of the model. The equivalent nodal force applied to each node has been computed as the resultant of the IOP pressure (acting normal to the posterior surface of the patient-specific cornea used as reference) over the quadrilateral area surrounding the node. This area is the one enclosed by the polyline connecting the centres of each quadrilateral made of two pairs of fibrils belonging to the two families. It follows that the hinges are loaded with a point load directed normally to the anterior surface of the trusswork shell, thus with different intensity and orientation (figure 5*c*).

(a) solid model (b) trusswork model **(c)** trusswork model

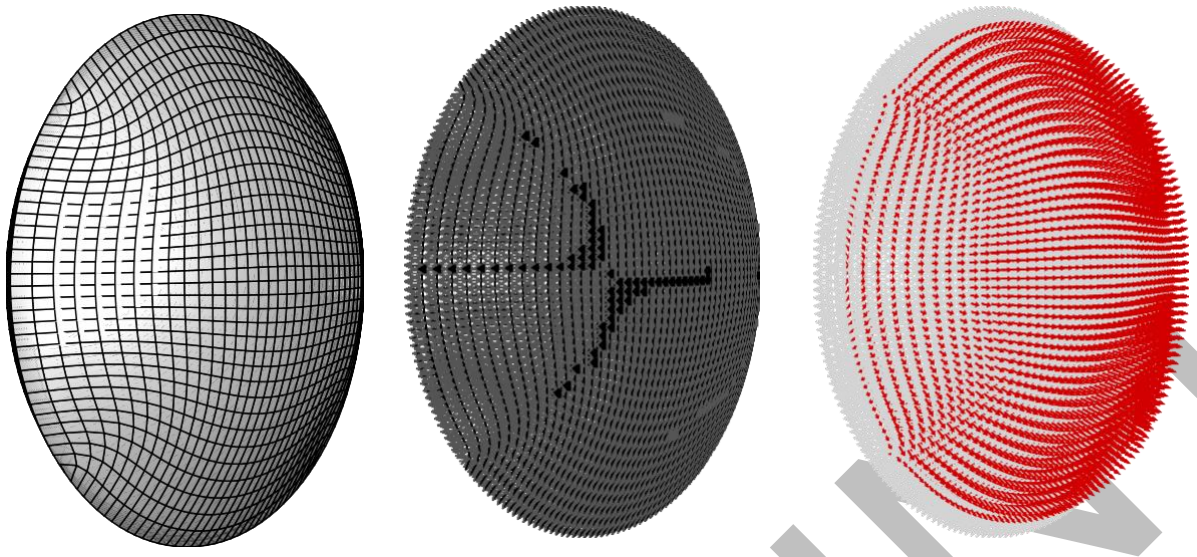

Figure 5. Model of the collagen structure used in the numerical simulations, comprising 5000 nodal points and 28 600 trusses. (a) Reference solid finite-element model used to define the geometry of the trusswork. (*b*) Full trusswork model including the five networks of elements (modelling fibrils and cross-links). (*c*) Point loads applied to the hinges of the network, representative of the action of the physiological IOP. (Online version in colour.)

Under the assumption of linearized elasticity, the static response of the trusswork to the action of the IOP is obtained in terms of nodal displacements as the solution of the linear system

$$\mathbf{KU} = \mathbf{F}, \tag{2.1}$$

where $\mathbf{K}$ is the stiffness matrix, $\mathbf{U}$ the unknown displacement array and $\mathbf{F}$ is the external load array that collects the point loads. From the linearized truss theory, the stiffness k_i of each truss is proportional to the young modulus E_i and to the area A_i of the cross section of truss. For the sake of simplicity, here we consider an equivalent rigidity parameter $D_i = E_i A_i$, and write for the truss stiffness

$$k_i = \frac{D_i}{h_i}, \tag{2.2}$$

where h_i is the length of the truss.

The choice of the values assigned to the stiffness parameters D_i of the model has been done on the basis of our sensitivity on the material parameters of the cornea acquired in previous works and from considerations on the structure of the stroma derived from literature data. In the cornea, collagen fibrils contribute considerably to sustain the physiological IOP (in average 15 mmHg). To estimate the overall contribution of collagen to the structural response, we considered finite-element calculations, conducted on the same geometry of the cornea considered here, by employing two different material models. The first model is a sophisticated anisotropic material model [31], featuring an isotropic matrix with a shear modulus $G = 0.05$ MPa (thus $E \approx 0.15$ MPa) and reinforcing fibres exhibiting an exponential behaviour. The second model is an isotropic material with Young modulus $E = 0.3$ MPa. At the physiological IOP both the models provided the apex displacement of 0.15 mm. By comparing the behaviours, we estimated that collagen fibrils contribute for about 50% of the corneal stiffness, i.e. we estimated the equivalent elastic modulus of the fibrils as $E_f = 0.15$ MPa. Correspondingly, the equivalent load of the simplified model must account only for the 50% of the physiological IOP (7.5 mmHg = 0.001 MPa).

The stiffness of trusses representative of the fibrils was estimated as an equivalent measure derived by homogenizing the contribution of the fibrils over a reference area. Since each truss must represent the behaviour of an area of the corneal section equivalent to $A_f = tux$, where $t = 0.3$ mm is the cornea thickness and $ux = 0.2$ mm is the mesh size, we estimated the equivalent rigidity of a fibril truss as $D_F = E_f A_f = 0.009$ N.

Table 1. List of rigidity material properties D_i, equivalent to dimensionless forces: values and ranges used in calculations. D_{F1} and D_{F1} refer to the twosetsof fibrils, D_{C1} and D_{C2} to the inter-cross-links of sets F1 and F2, respectively, and D_{C12} to the intra-cross-links between the two sets.

case	analysis	D_{F1}	D_{F2}	D_{C1}	D_{C2}	D_{C12}
1	healthy	1.00	1.00	0.80	0.80	0.5000
2	limbus	0.90	0.90	0.72	0.72	0.4500
	conus	0.01	0.01	0.01	0.01	0.0045
3	limbus	0.90÷0.40	0.90÷0.40	0.80	0.80	0.50÷0.2500
	conus	0.50÷0.25	0.50÷0.25	0.40	0.40	0.25÷0.0750
4	limbus	0.90÷0.40	0.90÷0.40	0.80÷0.20	0.80÷0.20	0.5000÷0.1000
	conus	0.80÷0.30	0.80÷0.30	0.70÷0.10	0.70÷0.10	0.0500÷0.0100
5	limbus	0.90÷0.40	0.90÷0.40	0.80÷0.20	0.80÷0.20	0.5000÷0.1000
	conus	0.80÷0.30	0.80÷0.30	0.70÷0.10	0.70÷0.10	0.0100÷0.0010
6	limbus	0.90÷0.40	0.90÷0.40	0.80÷0.20	0.80÷0.20	0.5000÷0.1000
	conus	0.80÷0.30	0.80÷0.30	0.70÷0.10	0.70÷0.10	0.002÷0.0001

The stiffness of the trusses representative of the intermolecular covalent cross-links that connect fibrils of the same or different families was estimated on the basis of experimental data. According to well-established multiscale theoretical framework specifically formulated for collagen in soft biological tissues [32], the experimentally measured stiffness of a filament of cross-link bond can be evaluated as $k_C = 5$ nN μm^{-1}. The centre to centre distance h between two fibrils in the stroma is ≈60 nm [33]; thus the force transmitted by a cross-link filament is $F_C = 0.3$ nN. To evaluate the number of cross-links N_c across the area A_f, we considered the typical spacing $d \approx 60$ nm between cross-link ropes along collagen fibrils [34] and, again, the separation h between two fibrils, obtaining $N_C = A_f/hd = 17 \times 10^6$. Thus, the equivalent rigidity of a cross-link truss is estimated as $D_C = F_C N_C = 0.0051$ N. To differentiate between the two types of cross-link in the model we considered the inter-cross-link slightly stiffer (0.0072 N) than the intra-cross-link (0.0045 N). The stiffness of the components of the trusswork has been normalized with respect to the stiffness of the fibril truss, obtaining the values $D_{F1} = D_{F2} = 1$, $D_{C1} = D_{C2} = 0.8$, $D_{C12} = 0.5$, reported in row 1 of table 1. The physiological IOP normalized with the same stiffness was set 0.1.

The use of the force-like stiffness (equivalent to Young's modulus by area) is due to desire to reduce the number of parameters to be considered in the analysis. The reduction of the equivalent stiffness accounts simultaneously for the reduction on the number of fibrils or cross-link and for the reduction of Young's modulus. This is indeed in keeping with the experimental observation that revealed that in keratoconus stroma cross-links weakens their stiffness and reduce in number [6].

In the case of a healthy cornea, we assign a uniform rigidity to all the elements of the same set, see case 1 in table 1. To model keratoconus, we make the assumption that the stiffness of both fibrils and cross-links reduces smoothly in the radial direction from the limbus, where it reaches its maximum value, to the centre of the conus, where it reaches its minimum value. Laking of direct suggestions derived from clinical observations, we consider three functional forms of material stiffness variation: linear, quadratic and cubic, respectively. The three distributions, shown in figure 6, provide a different extension of the diseased zone: while linear and cubic variations define a confined area of reduced stiffness, the quadratic variation defines a rather extended diseased area, which suggests a more pronounced propensity to deform. According to clinical observations, in most cases the centre of a keratoconus lesion is not located at the apex of the

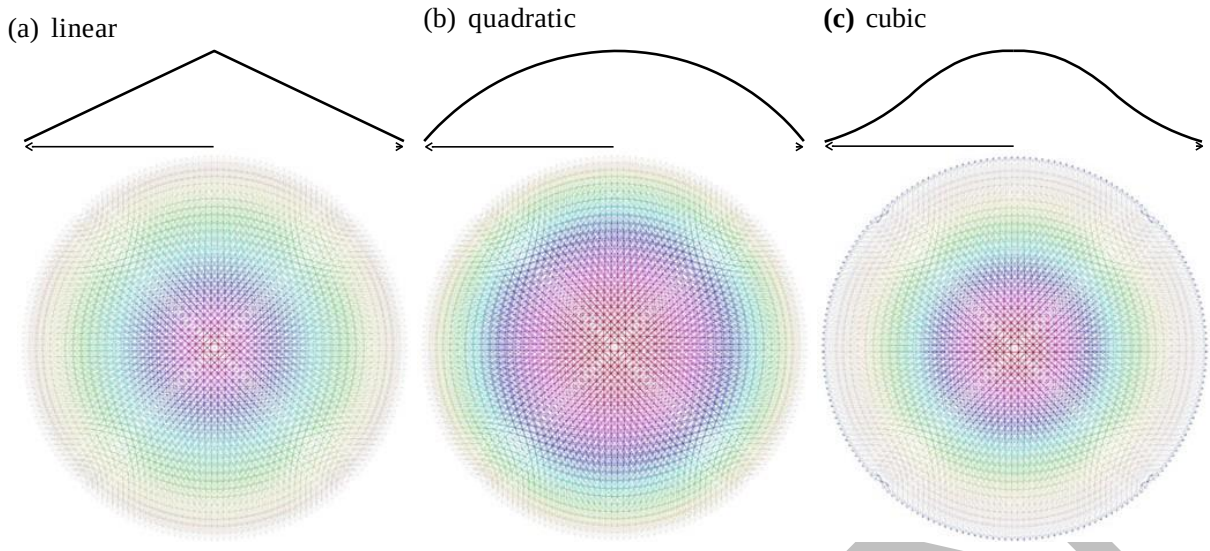

Figure 6. Variation of the material properties to model the reduction of the stiffness typical of keratoconus, characterized by a gradient of stiffness from the limbus to the centre of the conus. The light colour indicates a healthy material, the dark colour indicates a diseased material. Linear and cubic distributions of the material properties lead to a confined fully diseased zone, while the quadratic distribution produces a larger weakened zone that is more prone to deform.

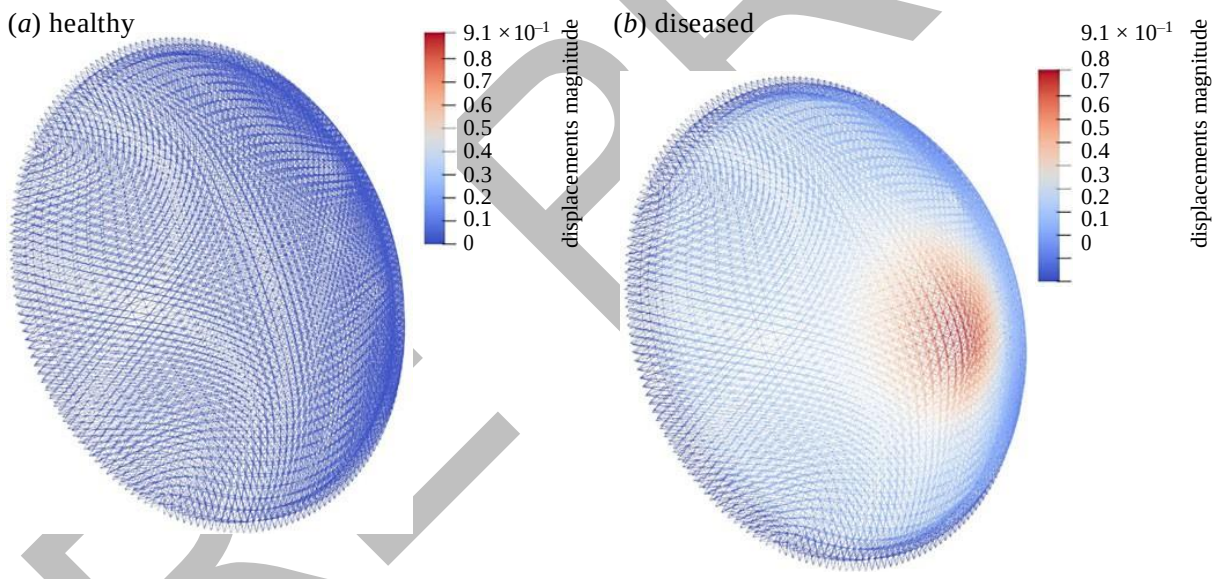

Figure 7. Example of output of the numerical calculations, equation 2.1. Colours map the displacement field, for the cases of (*a*) healthy cornea; (*b*) keratoconus cornea.

cornea, but along the SI meridian towards the inferior limbus. Therefore, we consider centres of the conus displaced from the corneal apex (see figure 9*a*).

3. Results

The smooth reduction of stiffness of the components allows one to model the protrusion of keratoconus. Figure 7 shows the results of two static analyses conducted for (*a*) a healthy cornea (material constants listed as case 1 in table 1) and (*b*) a diseased cornea (material constants listed as case 2 in table 1 with quadratic variation from limbus to conus). The centre of the conus is displaced 1 mm from the corneal apex. The colours map the displacement field, which is rather uniform for the healthy cornea while it protrudes in a conical shape for the keratoconus cornea.

Using this simple model, we conducted an intense programme of numerical calculations with the objective of assessing the relevance of the various components (fibrils and cross-links) on the

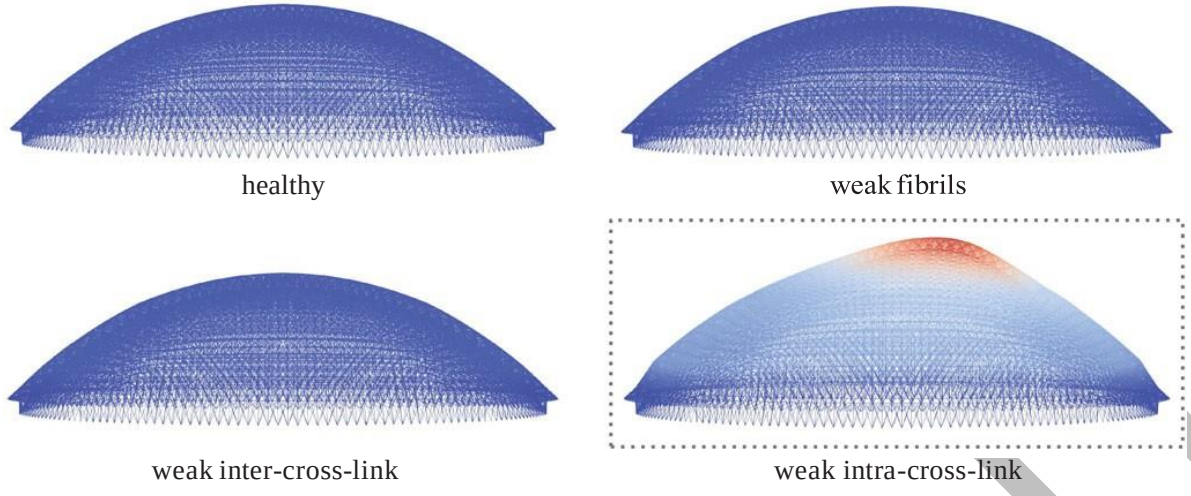

Figure 8. Relevance of the reduction of the stiffness of the individual components of the network on the formation of the conus. Comparison of the deformed shape and displacement field between an healthy cornea, a cornea weakened only in the F1 and F2 fibril stiffness, a cornea weakened only in the C1 and C2 cross-link stiffness, and a cornea weakened only in the C12 cross-link stiffness. The colour map refers to figure 7.

stability of the network, considering, in particular, the conditions that lead to the formation of an evidently protruding conus.

We begin with a factorial experiment considering the variation of the stiffness of each group of components of the network (fibrils F1 and F2, inter-cross-link C1 and C2, and intra-cross-link C12), within the ranges listed as case 3 in table 1. The study includes 28 764 analyses. Numerical results reveal that, as far as the conical shape is concerned, the most influential parameter is the stiffness of the intra-cross-link stiffness C12. The reduction of the stiffness of the fibrils (F1 and F2) without a corresponding reduction of the intra-cross-link stiffness C12 does not lead to a conical shape. Moreover, a reduction of the inter-cross-link stiffness C1 and C2 does not lead to any significant modification of the spherical shape.

Figure 8 visualizes the NT sections of four significant cases. The first image corresponds to a healthy cornea, with stiffness parameters listed as case 1 in table 1. The colours map the displacement field with the same scale reported in figure 7. The second image corresponds to a weaker structure, where the stiffness of the F1 and F2 fibrils has been reduced according to case 2 in table 1, while the stiffness of the cross-links is kept equal to the ones in case 1. The third image corresponds to another weaker structure, where the stiffness of the C1 and C2 cross-links has been reduced according to case 2 in table 1, while the stiffness of the fibrils and of the intra-cross-links is kept equal to the ones in case 1. The fourth image (framed) corresponds to a structure where only the C12 cross-link stiffness is reduced according to case 2, while the other parameters are kept equal to the ones in case 1. Clearly, the only case where the structure deforms forming a conus, leading to diversified displacement field, is the one characterized by the weakening of the C12 bonds.

We continue by illustrating the synthetic results of the search of the optimal functional form of the distribution (i.e. the spatial gradient) of material stiffness as the one able to produce the most realistic shape for the keratoconus. These analyses include the investigation on the location of the centre of the lesion, which affects the global shape of the conus. We consider three positions for the centre of the lesion: at the corneal apex, and 1 mm and 2 mm displaced from the apex (figure 9*a*). Figure 9 compares the deformed shapes of the cornea for three different positions of the conus centre and for the three functional forms of the stiffness distribution. As anticipated, the linear distribution leads to a very localized deformation, figure 9*b*; a cubic distribution does involve a larger zone but the size of the conus is still limited and not realistic, figure 9*d*; while the quadratic distribution, figure 9*c*, produces a protrusion that resembles the ones documented in clinical observations.

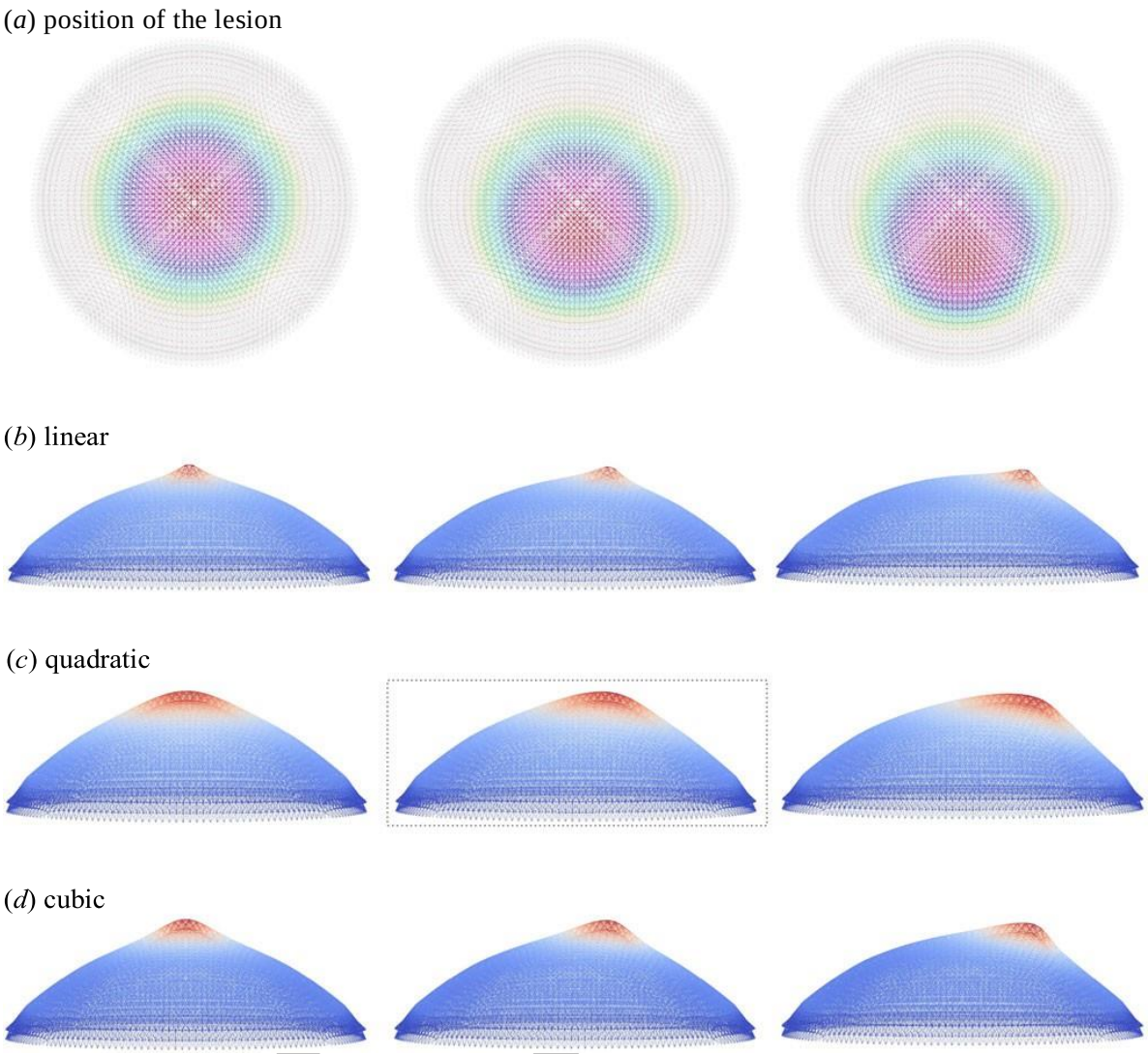

Figure 9. Influence of the location of the centre of the lesion and of the distribution of the material properties reduction on the shape of the keratoconus. (*a*) Visualization of the material properties for three lesions, centred at the corneal apex, and 1 mm and 2 mm away from the apex along the SI meridian. The colours map the variation of the material stiffness. (*b*) Shape of the conus obtained with the assumption of linear variation of the material properties from limbus to conus. (*c*) Shape of the conus obtained with the assumption of quadratic variation of the material properties from limbus to lesion centre. (*d*) Shape of the conus obtained with the assumption of cubic variation of the material properties from limbus to lesion centre. In (*b–d*), the colours map the displacement field.

Figure 10. Comparison of the shape of (*a*,*b*) clinically observed keratoconus corneas and (*c*) numerically obtained deformed geometry. The two clinical images have been downloaded from the web.

Figure 10 shows a qualitative comparison between clinical images and the prediction of the numerical model.

Figure 11 illustrates the influence of the stiffness of the intra-cross-link (C12). Specifically, figure 11*a* shows the dependence of the magnitude of the conical protrusion on the distribution of the stiffness of the C12 bonds, considering three different positions of the centre of the lesion. Plots

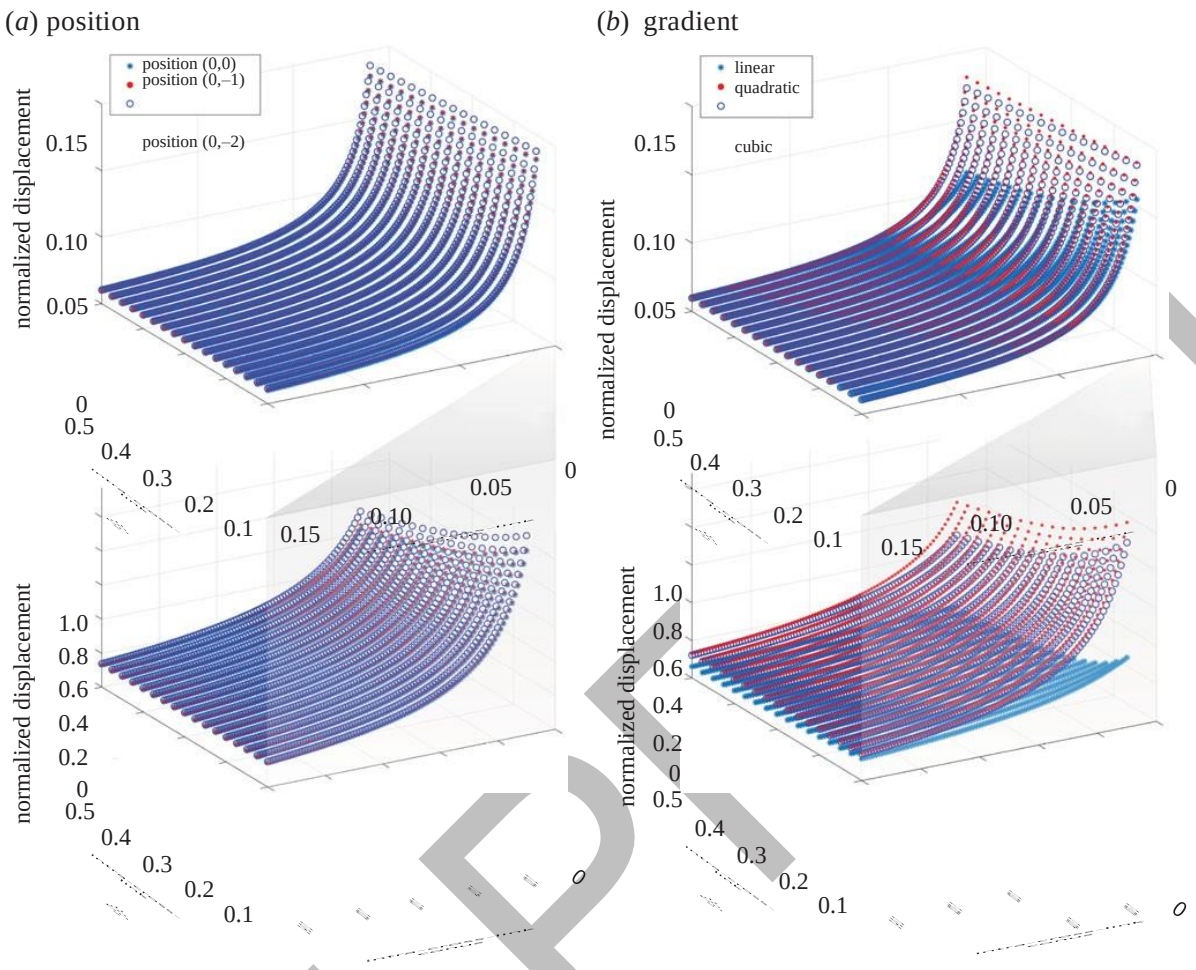

Figure 11. Synthesis of the most meaningful results of 7191 combinatory analyses where the stiffness of the intra-cross-link (both at limbus and at the centre of the lesion, where the apex of the keratoconus is located) is varied: effects on the maximum protrusion of the conus. Top images refer to a larger range of the lesion stiffness; bottom images refer to a narrower range of the lesion stiffness. (*a*) Influence of the position of the centre of the lesion. (*b*) Influence of the functional form of the distribution of the material stiffness around the centre of the lesion.

indicate that the relevance of the stiffness of the intra-cross-link at limbus is minimal; moreover, the actual position of the lesion is not particularly influential on the final shape. Figure 11*b* shows the dependence of the conus protrusion on the functional forms of the distribution of the stiffness around the lesion. The second row shows a refined analysis on the intra-cross-link conus axis. Plots confirm the observations drawn for figure 11*a*. In particular, for all the combination of parameters, the quadratic distribution of the stiffness produces the largest displacements.

According to the results of the first set of analyses, we conduct a more detailed investigation for the case of the conus dislocated 1 mm from the corneal apex with a quadratic distribution of the material properties (see the framed keratoconus in figure 9). The extensive factorial experiment comprises 150 280 simulations where we combine the stiffness of the components of the network. Each stiffness varies within the range reported under the cases 4, 5 and 6 in table 1. We remark that cases 4, 5 and 6 differ only for the width of the range of variability of the intra-cross-link C12 at the centre of the lesion. A synthesis of the results of this parametric study is reported in figure 12, in terms of maximum displacement of the apex of the keratoconus. The protrusion magnitude is plotted versus the stiffness of the intra-cross-link sets, at the limbus and at the centre of the lesion, for different combinations of the stiffness of the F1, F2, C1 and C2 components. The graphs on the left side, figure 12*a*, describe a cornea with a mild disease, where the stiffness of the fibre sets F1 and F2 at limbus is assumed to remain high. The graphs on the right side, figure 12*b*,

describe a cornea with a severe disease, characterized by a marked reduction of the stiffness of the fibre sets F1 and F2 at the limbus. Each graph reports five sets of data, corresponding to the selected combinations of the stiffness of the network components, see the caption of figure 12 for the description of the legend key. Plots show that the conus protrusion is enhanced when the inter-cross-link (C1 and C2) and intra-cross-link (C12) stiffness decrease below 1% of the reference

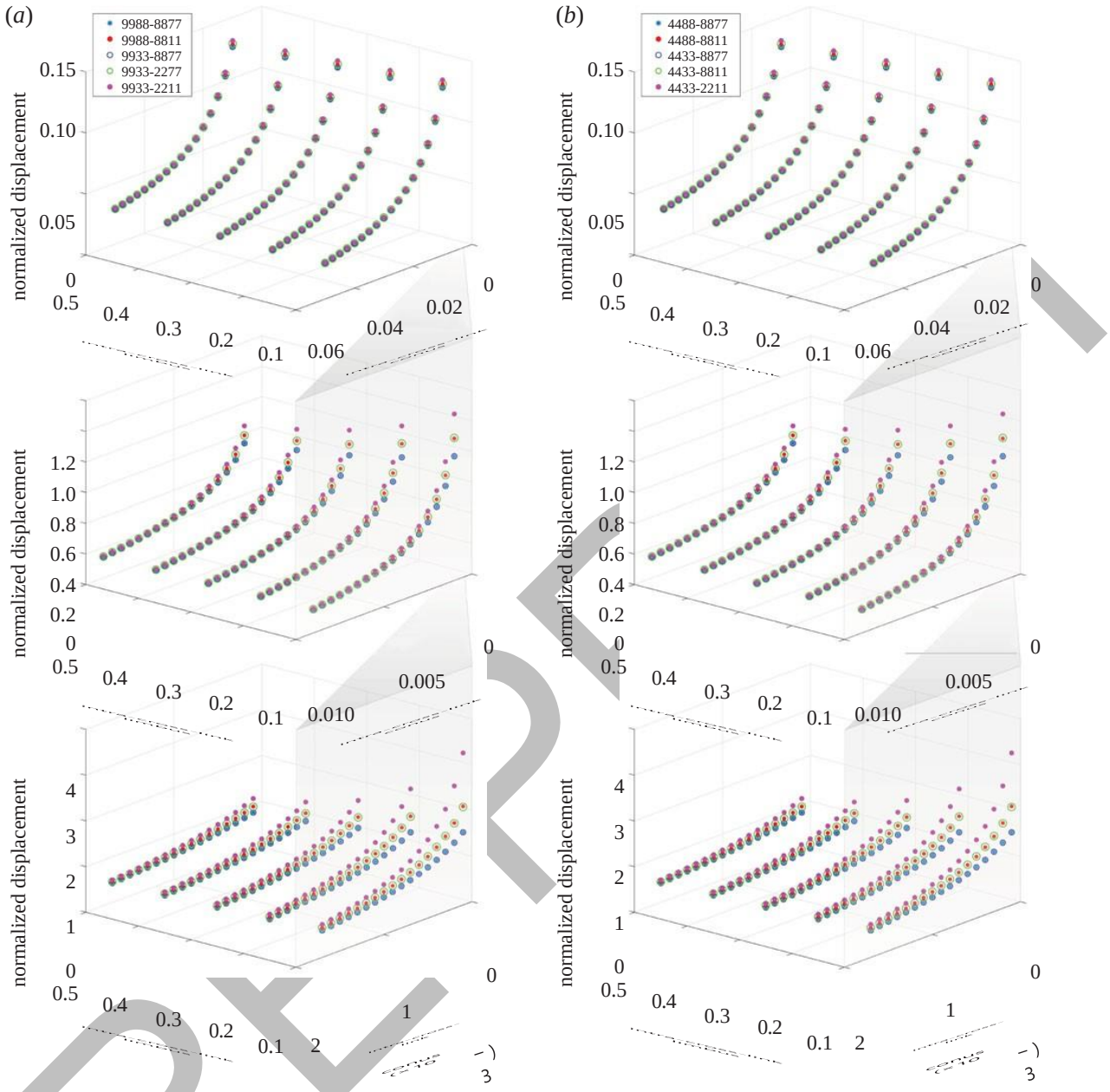

Figure 12. Dependence of the maximum protrusion of the conus on the stiffness of the components of the network for a selection of the performed analysis. Left plots visualize the dependence on various stiffness values for a cornea characterized by a rather stiff limbus, associated to a mild keratoconus. Right plots visualize the same kind of dependence for cornea characterized by a soft limbus, associated to a severe keratoconus. From top to bottom, plots show the results for a progressively narrowed range of the intra-cross-link stiffness, see cases 4, 5 and 6 in table 1. The form XYZW-xyzw of the legend key has the following meaning. The first four numbers XYZW denote the stiffness of the network components at limbus. The second four numbers xyzw denote the stiffness of the network components at the centre of the lesion. X and x are the stiffness of the F1 sets, Y and y of the F2 sets, Z and z of the C1 sets, and W and w of the C2 set. All stiffness in the key are expressed in tenths of the stiffness of the F1 set of a healthy cornea, see case 1 in table 1.

stiffness. This observation has been confirmed by numerous other results, not shown here for the sake of brevity. The feeling drawn from these analysis is that the mechanical stability of the collagen in the cornea is guaranteed by the presence of cross-links. The weakening of the cross-links, independently of the physical reason that causes the degradation, may justify the loss of

stability with the formation of a conical protrusion.

4. Discussion

This study has been carried on with two goals: (i) to understand the importance of the explicit description of the cross-links between the two sets of main fibrils in a microstructural model of the

collagen reinforcement of the human cornea; (ii) to identify the components of the network whose failure is connected to the bulging observed in corneal ectasia and keratoconus. Thus the study focuses on the structural aspects of the network of fibrils of the stroma and on the mechanical conditions that compromise the stability of the corneal shell, and do not tackle the actual causes (chemical, mechanical and inflammatory) that trigger the disease.

We propose a very simplified model of the reinforcement of the cornea, which nevertheless includes the reinforcing fibrils and bonds (cross-links) that are observed in diagnostic images of the cornea. We hypothesize an organization of the fibrils that reflects the ophthalmologic observations, characterized by an orthogonal NT–SI pattern at the centre of the cornea and a circumferential–radial pattern at limbus. We note that this organization is universally acknowledged by the scientific community and is implemented in the most advanced numerical models of the cornea [14,15,18,20,26,31]. From a structural point of view, the simple orthogonal arrangement of two sets of independent fibrils F1 and F2 is not stable, figure 3*a*. Bonds between the fibrils of the same set, or inter-cross-link C1 and C2, are introduced to model the highest level structures called lamellae (figure 3*b*). The two resulting macro-lamellae are not connected and the structure is not able to sustain the point loads that mimic the IOP. The structure becomes stable by introducing additional bonds, or intra-cross-link, between the two sets of fibrils (C12) with a crossing pattern that sustains the transversal loads. These bonds play the role of the actual cross-links of the stroma that allow the lamellae to maintain a precise distribution to assure a uniform degree of rigidity to the cornea. Thus, the main features of the collagen architecture of the stroma are included in the model.

We note that in a continuum model with embedded fibres used for simulation of the biomechanics of a normal cornea it is not necessary to include cross-link bonds since the stabilization function is accomplished by the matrix. Obviously, in a continuum model is also impossible to model the deficiency of selected elements of a microstructure that may lead to ectasia or keratoconus.

We selected a patient-specific shape of the cornea to achieve a more realistic model of the keratoconus. For the same reason, we assigned a thickness to the model, although for a suitable selection of the material stiffness the structure is sufficiently robust to support the point loads representing the IOP. The choice of a 0.3 mm thickness instead of the more realistic average value of 0.5 mm is done with the goal to enhance the conical shape in diseased cornea models. In our experiments, indeed, thicker corneas formed smoother protrusions as a consequence of the increased stiffness, in line with typical behaviours of thin spatial reticular structures used, e.g. in civil engineering.

The distribution of the stiffness of the trusses in keratoconus models deserves a comment. In a first attempt to model the bulging of the tissue, we followed [15] where the conus was described as two concentric regions with reduced material stiffness: the central one with no fibres, thus described as a Mooney–Rivlin isotropic material, and the periphery region with reduced values for the fibre stiffness. The bi-material description of the lesion, which worked rather well in continuum models, is not appropriate for the trusswork structure since it leads to unrealistic localization of the deformations at the boundaries of the two concentric regions. The introduction of a smooth gradient for the distribution of the stiffness solved the problem.

We remark that, by reducing the stiffness of all the components at the same time, or only the stiffness of the fibrils D_{F1} and D_{F2}, the model produces a spherical shape which is unable to capture the typical conus of a diseased eye. The reduction of the stiffness of the cross-link D_{C1} and D_{C2} is very marginally relevant on the final shape. Finally, the apparently drastic decrease of the values of stiffness D_{C12} with respect to the other parameters does correspond to the exclusion of the contribution of these trusses to the stability of the structure. The complete removal of these trusses is indeed precluded by the model, because it will result in an under-determined structure, and the corresponding stiffness matrix will be singular.

In spite of the apparent simplicity, the model here proposed is able to reproduce the mechanism of bulging of the cornea that is observed in pathologies like the keratoconus. The model accounts for the micro-components of the structure of the stroma and allows one to assess the relevance

of each component on the global stability of the structure. As a micromechanical model, it is in line with the most advanced approaches that are currently developed to provide an explanation for material degeneration [35]. To our knowledge, however, no microstructural study has been conducted on the collagen of the cornea, in contrast with the large use of trusswork domes in civil engineering [36], in biology [37] and in chemistry [38].

The simplicity of the structural model and the reduced number of parameters suggested to conduct a simple parametric analysis by spanning the range of values of interest. We realized that there was no need to use analysis of variance or analysis of regression since the relevance of the intra-cross-link parameter appeared immediately dominant over the others.

Results of an extended parametric analysis have confirmed that the structural elements most influential on the development of a conical shape of the structure are the intra-cross-link (C12) bonds, which are fundamental for the global stability of the structure. This is interestingly related to clinical observations. Clinical evidence has revealed that keratoconus tissue is characterized by a randomness in the distribution of the fibrils that is unusual in healthy corneas. Apparently, the lamellae are still present but they are not able to confine uniformly the IOP. This is likely due to the absence of chemical bonding between the lamellae [5,6]. To reflect the actual collagen structure of the cornea, the stiffness of the fibrils F1 and F2 must be larger than the one of the cross-links since fibrils are the strongest structures of the stroma. Inter-cross-link bonds C1 and C2 show in general a second order influence, since their stabilization function becomes important only for low values of the inter-cross-link stiffness C12.

The relevance of the weakening of the C12 diagonal links on the development of the keratoconus has been verified here numerically, by running thousands combinations of values, just not to leave any case untried. However, the result was expected, since it is an obvious consequence of the trusswork theory. Indeed, any square design trusswork with missing diagonal struts or tie-rods is statically unstable. Only when diagonal elements are introduced, the trusswork is able to adsorb all the loads, showing a remarkable stiffness with a very moderate deformation, and a very low weight/stiffness ratio. This particularly advantageous property justifies the diffusion of trussworks or tensegrity networks in many fields of civil, mechanical, and aeronautical engineering, and explains the large presence of trusswork-like structures in biology (bones, tree leaves, silicon-based diatomeae, just to mention a few examples).

The particular discretization of the model has been inherited from the successful finite-element design of the cornea developed in [15] and carries the following drawback. Trusses modelling fibrils and cross-links located in proximity of the limbus are geometrically longer than others and, according to (2.2), are more compliant than other elements of the structure. Thus, the material stiffness D_i of the C12 elements at limbus cannot be reduced as much as the one at the centre of the lesion, because the global shape of the cornea would be unrealistic. Interestingly this drawback is of scarce relevance for the proposed model, since a marked reduction of the stiffness of the limbus, the thickest and strongest portion of the cornea, is not realistic.

In principle, the model could be used to simulate other loading conditions, e.g., idealized contact and non-contact tonometry tests, but, under the linearized kinematic assumption here considered, the mechanical response would not be realistic. In general, the applicability of the present model to the simulation of any *in vivo* test is questionable, since the description of the sole reinforcing structure is way too far from representing the behaviour of the complex corneal tissue. The model is intended to reproduce the typical physiological behaviour of the carrying structure cornea, and, in particular, for its specific features is not proper to be used in the simulation of the air puff test since there is no differentiation between tensile and compressive behaviour.

Nevertheless, the study clarifies the structural functions of the collagen links and the suggestions drawn from the results can be used to improve existent models of the cornea. In the limits of approximation offered by the present model, the suggestion that we obtain from this study is that from the structural point of view the keratoconus is the result of the weakening of intra-fibrillar bonds. The numerous simplifying assumptions used in the creation of the trusswork rule out any predictive capacity of the model, that cannot be used directly for quantitative estimates.

In particular, the collagen structure here presented fully disregards the elastin and proteoglycan matrix, and therefore it fails to be representative of the actual behaviour of the stroma. As a matter of fact, the collagen structure is immersed in a deformable medium and connected to it by chemical bonds that allow the interaction between fibrils and matrix.

In the view of the creation of a predictive model of the human stroma, the collagen structure should be connected to the elastic matrix by classical methods of computational mechanics; for example, (i) adopting homogenization techniques, where the structure is embedded into a homogenized material that preserves the features of the microstructure, making use of generalized tensors or pseudo-invariants [26]; or (ii) using superposition techniques where structural and continuum elements are combined as it is done in modelling steel bars in reinforced concrete. A more challenging task is the direct inclusion of the collagen structure in micromechanical models of the cornea, which opens the possibility to account for other physics to describe the material degradation and explain the weakening of the bond stiffness [39]. In this sense, interesting suggestions can be taken from models of cell mechanics [40,41].

Data accessibility. This article has no additional data.

Authors' contributions. A.P. wrote the software and drafted the manuscript. A.G. performed the data analysis. M.V. organized the results and completed the manuscript. All authors read and approved the manuscript.

Competing interests. We declare we have no competing interests.

Funding. No funding has been received for this article.

References

1. Buzard KA. 1992 Introduction to biomechanics of the cornea. *Refract. Corneal Surg.* **8**, 127–138.
2. Meek KM, Boote C. 2009 The use of X-ray scattering techniques to quantify the orientation and distribution of collagen in the corneal stroma. *Prog. Retin. Eye Res.* **28**, 369–392. (doi:10.1016/j.preteyeres.2009.06.005)
3. Rabinowitz YS. 1998 Keratoconus. *Surv. Ophthalmol.* **42**, 297–319. (doi:10.1016/S0039-6257(97) 00119-7)
4. Ambekar R, Toussaint KC, Johnson AW. 2011 The effect of keratoconus on the structural mechanical, and optical properties of the cornea. *J. Mech. Behav. Med. Biomater.* **4**, 223–236. (doi:10.1016/j.jmbbm.2010.09.014)
5. Huang Y, Tuft SJ, Meek M. 1996 Histochemical and X-ray diffraction study of keratoconus epikeratoplasty. report of two cases. *Cornea* **15**, 320–328. (doi:10.1097/00003226-199605000- 00016)
6. Daxer A, Fratzl P. 1997 Collagen fibril orientation in the human corneal stroma and its implication in keratoconus. *Invest. Ophthalmol. Vis. Sci.* **38**, 121–129.
7. Price FW, Price MO. 2005 Descemet's stripping with endothelial keratoplasty in 50 eyes: a refractive neutral corneal transplant. *J. Refract. Surg.* **21**, 339–345. (doi:10.3928/1081-597X-20050701-07)
8. Hellstedt T, Mäkelä J, Uusitalo R, Emre S, Uusitalo R. 2005 Treating keratoconus with intacs corneal ring segments. *J. Refract. Surg.* **21**, 236–246.
9. Melles GRJ, Lander F, Rietveld FJ, Remeijer L, Beekhuis WH, Binder PS. 1999 A new surgical technique for deep stromal, anterior lamellar keratoplasty. *Br. J. Ophthalmol.* **83**, 327–333. (doi:10.1136/bjo.83.3.327)
10. Wollensak G, Spoerl E, Seiler T. 2003 Stress-strain measurements of human and porcine corneas after riboflavin-ultraviolet-a-induced cross-linking. *J. Cataract Refract. Surg.* **29**, 1780–1785. (doi:10.1016/S0886-3350(03)00407-3)
11. Baiocchi S, Mazzotta C, Cerretani D, Caporossi T, Caporossi A. 2009 Corneal crosslinking: riboflavin concentration in corneal stroma exposed with and without epithelium. *J. Cataract Refract. Surg.* **35**, 893–899. (doi:10.1016/j.jcrs.2009.01.009)
12. Petsche SJ, Chernyak D, Martiz J, Levenston ME, Pinsky PM. 2012 Depth-dependent transverse shear properties of the human corneal stroma. *Invest. Ophthalmol. Vis. Sci.* **53**, 873–880. (doi:10.1167/iovs.11-8611)

13. Abass A, Hayes S, White N, Sorensen T, Meek KM. 2015 Transverse depth-dependent changes in corneal collagen lamellar orientation and distribution. *J. R. Soc. Interface* **12**, 20140710. (doi:10.1098/rsif.2014.0717)
14. Pinsky PM, van der Heide D, Chernyak D. 2005 Computational modeling of mechanical anisotropy in the cornea and sclera. *J. Cataract Refract. Surg.* **31**, 136–145. (doi:10.1016/j.jcrs.2004.10.048)
15. Pandolfi A, Manganiello F. 2006 A material model for the human cornea. *Biomech. Model. Mechanobiol.* **5**, 237–246. (doi:10.1007/s10237-005-0014-x)
16. Pandolfi A, Holzapfel GA. 2008 Three-dimensional modelling and computational analysis of the human cornea considering distributed collagen fiber orientation. *J. Biomech. Eng.* **130**, 061006. (doi:10.1115/1.2982251)
17. Pandolfi A, Fotia G, Manganiello F. 2009 Finite element simulations of laser refractive corneal surgery. *Eng. Comput.* **25**, 15–24. (doi:10.1007/s00366-008-0102-5)
18. Sánchez P, Moutsouris K, Pandolfi A. 2014 Biomechanical and optical behavior of human corneas before and after photorefractive keratectomy. *J. Cataract Refract. Surg.* **40**, 905–917. (doi:10.1016/j.jcrs.2014.03.020)
19. Simonini I, Pandolfi A. 2015 Customized finite element modelling of the human cornea. *PLoS ONE* **10**, e0130426. (doi:10.1371/journal.pone.0130426)
20. Ariza-Gracia MA, Zurita JF, Piñero DP, Rodriguez-Matas JF, Calvo B. 2015 Coupled biomechanical response of the cornea assessed by non-contact tonometry. A simulation study. *PLoS ONE* **10**, e0121486. (doi:10.1371/journal.pone.0121486)
21. Roy AS, Kurian M, Matalia H, Shetty R. 2015 Air-puff quantification of non-linear biomechanical properties of the human cornea in vivo. *J. Mech. Behav. Med. Biomater.* **48**, 173–182. (doi:10.1016/j.jmbbm.2015.04.010)
22. Simonini I, Pandolfi A. 2016 The influence of intraocular pressure and air jet pressure on corneal contactless tonometry tests. *J. Mech. Behav. Med. Biomater.* **58**, 75–89. (doi:10.1016/j.jmbbm.2015.07.030)
23. Simonini I, Angelillo M, Pandolfi A. 2016 Theoretical and numerical analysis of the corneal air puff test. *J. Mech. Phys. Solids* **93**, 118–134. (doi:10.1016/j.jmps.2016.04.012)
24. Ariza-Gracia MA, Redondo S, Pinero Llorens D, Calvo B, Rodriguez Matas JF. 2017 A predictive tool for determining patient-specific mechanical properties of human corneal tissue. *Comput. Methods Appl. Mech. Eng.* **317**, 226–247. (doi:10.1016/j.cma.2016.12.013)
25. Rivlin RS, Saunders DW. 1951 Large elastic deformations of isotropic materials. VII. Experiments on the deformation of rubber. *Phil. Trans. R. Soc. Lond. A* **243**, 251–288. (doi:10.1098/rsta.1951.0004)
26. Studer H, Larrea X, Riedwyl H, B"uchler P. 2010 Biomechanical model of human cornea based on stromal microstructure.*J. Biomech.* **43**, 836–842. (doi:10.1016/j.jbiomech.2009.11.021)
27. Gefen A, Shalom R, Elad D, Mandel Y. 2009 Biomechanical analysis of the keratoconic cornea. *J. Mech. Behav. Med. Biomater.* **2**, 224–236. (doi:10.1016/j.jmbbm.2008.07.002)
28. Roy AS, Dupps Jr WJ. 2011 Patient-specific computational modeling of keratoconus progression and differential responses to collagen cross-linking. *Invest. Ophthalmol. Vis. Sci.* **52**, 9174–9187. (doi:10.1167/iovs.11-7395)
29. Lago MA, Rupérez MJ, Monserrat C, Martínez-Martínez F, Martínez-Sanchis S, Larra E, Díez-Ajenjo MA, Peris-Martínez C. 2015 Patient-specific simulation of the intrastromal ring segment implantation in corneas with keratoconus. *J. Mech. Behav. Biomed. Mater.* **51**, 260–268. (doi:10.1016/j.jmbbm.2015.07.023)
30. Aghamohammadzadeh H, Newton RH, Meek KM. 2004 X-ray scattering used to map the preferred collagen orientation in the human cornea and limbus. *Structure* **12**, 249–256. (doi:10.1016/j.str.2004.01.002)
31. Montanino A, Gizzi A, Vasta M, Angelillo M, Pandolfi A. 2018 Modeling the biomechanics of the human cornea accounting for local variations of the collagen fibril architecture. *ZAMM - J. Appl. Math. Mech.* **98**, 2122–2134. (doi:10.1002/zamm.v98.12)
32. Marino M, Vairo G 2013 Multiscale elastic models of collagen bio-structures: From cross-linked molecules to soft tissues. In Multiscale Computer Modeling in Biomechanics and Biomedical Engineering. Studies in Mechanobiology, Tissue Engineering and Biomaterials, vol. 14 (ed. A Gefen), pp. 73–102. Berlin, Germany: Springer.

33. Gyi TJ, Meek KM, Elliott GF Collagen interfibrillar distances in corneal stroma using synchrotron X-ray diffraction: a species study. *Int. J. Biol. Macromol.* **10**, 265–269. (doi:10.1016/0141-8130(88)90002-5)
34. Scott JE. 2003 Elasticity in extracellular matrix 'shape modules' of tendos, cartilage, etc. a sliding proteoglycan-filament model. *J. Physiol.* **553**, 335–343. (doi:10.1113/jphysiol.2003.050179)
35. Marino M, Vairo G. 2014 Influence of inter-molecular interactions on the elasto-damage mechanics of collagen fibrils: a bottom-up approach towards macroscopic tissue modeling. *J. Mech. Phys. Solids* **73**, 38. (doi:10.1016/j.jmps.2014.08.009)
36. Shea K, Cagan J. 1997 Innovative dome design: applying geodesic patterns with shape annealing. *AI EDAM* **11**, 379–394. (doi:10.1017/S0890060400003310)
37. Entcheva E, Bien H. 2009 Mechanical and spatial determinants of cytoskeletal geodesic dome formation in cardiac fibroblasts. *Integr. Biol.* **1**, 212–219. (doi:10.1039/b818874b)
38. Simmel SS, Nickels PC, Liedl T. 2014 Wireframe and tensegrity DNA nanostructures. *Accounts Chem. Res.* **47**, 1691–1699. (doi:10.1021/ar400319n)
39. Cyron CJ, Humphrey JD. 2017 Growth and remodeling of load-bearing biological soft tissues. *Meccanica* **52**, 645–664. (doi:10.1007/s11012-016-0472-5)
40. Humphries DL, Grogan JA, Gaffney EA. 2017 Mechanical cell–cell communication in fibrous networks: the importance of network geometry. *Bull. Math. Biol.* **79**, 498–524. (doi:10.1007/s11538-016-0242-5)
41. Müller KW, Cyron CJ, Wall WA. 2015 Computational analysis of morphologies and phase transitions of cross-linked, semi-flexible polymer networks. *Proc. R. Soc. A* **471**, 20150332. (doi:10.1098/rspa.2015.0332)